ISSN: 1687-1006 p
ISSN: 2682-3640 e

The Egyptian International Journal of Engineering Sciences and Technology

https://eijest.journals.ekb.eg/

Vol. 42 (2023) 38–44

DOI: 10.21608/eijest.2022.157438.1177

A Free Convection Heat Transfer Enhancement in A Vertical Channel Using Obstructions Inside The Channel

Sayed Ahmed E. Sayed Ahmed[a,*], Mohamed A. Essa[a], Mohamed Magdy Nouh[b]

[a] *Mechanical power department, Faculty of engineering, Zagazig University, 44519, Egypt.*
[b] *Egyption Ministry of Defense and Military Production, Mechanical power, Cairo, Egypt.*

ARTICLE INFO

Article history:

Received 20 August 2022
Received in revised form 11October 2022
Accepted 04 November 2022
Available online 04 November 2022

Keywords:

Heat transfer enhancement
free convection
Chimney effect
obstructions

ABSTRACT

A chimney system is combined of two heated plates with adiabatic extension. The numerical analysis of the chimney system is carried out to clarify the performance of the free convection heat transfer and the augmentation of mass flow rate (m•) for the tested parameters. A Computational fluid dynamic (CFD) software, ANSYS-FLUENT, is employed in this investigation. Itis found that there is good agreement between the numerical findings and the experimental data collected from the literature, as demonstrated by this validation. Two types of obstruction are used in the present investigation, which are rectangular and semi-circular. The two types are tested at different configurations. Results reveled that the obstructions reduce the velocity and form vortices, which led to the reduction of the mass flow rate. In addition, it is found that the highest (m•) is achieved with the base case However, the semi-circular chimney found to achieve the highest among obstructions.

1. Introduction

For natural air convection, a vertically heated channel (chimney) with adiabatic extensions at the top is considered as an effective option. This channel with a variety of designs is chosen in many applications, such as the cooling of electronic equipment by natural convection flows caused by the temperature differential between the nuclear reactor core and its surrounds [1,2].

Assuming that the chimney walls are adiabatic, the chimney system was heated symmetrically with a uniform heat flux (q") applied to the channel wall. For better heat transmission, chimney systems might be examined for optimal geometrical characteristics [5]. To determine the thermal performance of the heated channel without extension, numerical research was conducted [6]. Several distinct obstructions were introduced into the channel at various Ra values. Results indicated that the values of Nu rose with increasing Ra, and Nu values for the blocked channel were superior to those for the smooth one.

The thermal performance and fluid flow characteristics of a chimney system were investigated, experimentally, using various parameters [7]. The non-dimensional parameter ranges used in this investigation are as follows: $1.0 < B/b < 4.0$, $1.5 < L/Lh < 4.0$ and $10^2 < Ra < 10^6$.Results shown that modifying the geometrical parameters has a negligible impact on the local Nusselt number (Nux). Significant relationships were also discovered to be consistent with the experiments' conclusions. Different Ra ranges were studied in the same range of geometric characteristics [8]. Results demonstrated that the maximum and minimum wall temperatures increased with increasing aspect ratio (B/b) and constant Ra. Furthermore, the optimal value of B/b

* Corresponding author. Tel.: 01066325010
E-mail address: sahmeds@zu.edu.eg

depends mostly on Ra and L/Lh [9]. At $Ra=10^2$, the maximum value of Nu was found at B/b=4, while the lowest one was at B/b=1. In contrast, at $Ra=10^4$, B/b = 2 produced the greatest value of Nu, while B/b = 4 produced the smallest.

An asymmetrically heated chimney system was tested under a constant q" [10]. Increasing Lh/b increases thermal performance (wall temperature). Changing chimney height and diameter was experimentally and numerically studied [11]. Heat transfer rate rose with chimney height for all Pr. [12] investigated a vertical channel with a centerline auxiliary plate to increase heat and flow. The auxiliary plate is heated at $10^5 < Ra < 10^6$. Results showed that (m•) increased by inserting the heating of auxiliary plate. While the adiabatic one decreased the m•.

Inserting auxiliary plates between heated plates in the chimney system has been studied, both, experimentally and mathematically [13,14]. m• and thermal performance were shown to be affected. Two distinct methods were used to implant the auxiliary plate. A heated plate was put between the heated chimney sides in the first method. whereas the second was for an adiabatic system. When the auxiliary plate was heated, m• rose, but m• was reduced when the plate was adiabatically heated. Because of this, the heated auxiliary plate is the preferable option. In [15], the influence of a chimney on a heat sink's performance is examined. The use of a chimney enhances the airflow within a heat sink by 25%, regardless of the heat sink's height or depth.

Thermal performance was evaluated by [16] by placing a finned plate into the chimney The fins' heights and distances between them were examined. " At the maximum fin height and/or a small distance between fins, thermal performance increased. A generic model for solar chimneys has been developed, and findings have shown that this model and the collected data [17] have a good agreement. The influence of Ra on heat transmission can be discovered by [18]. Results demonstrated that pure conduction dominates heat transmission at low Ra, but as Ra increases, spontaneous convection takes over.

According to the above-mentioned reviews, it is necessary to comprehend what occurs inside the chimney system in order to pick appropriate settings leading to improved performance. In the current study, a numerical solution is performed to clarify the effect of different parameters on m• and Nu. Two types of obstructions were inserted inside the heated section to show its effect on the performance.

2. Model description

The present research paper is conducted numerically with validating data with experimental data obtained from [7]. The experimental model is shown in Fig.1. The channel is made of pairs of heated plates made from phenolic fiberboard 3.2 mm thick and 530 mm wide (Z-direction) with thermal conductivity equal to 0.17 W/m.K. The heater is wrapped over the outer surface of the channel. To reduce conductive heat losses, a polystyrene block with a thickness of 150 mm is attached to the back face of each plate for thermal insulation.

The chimney is made of two polystyrene plates with a thickness of 30 mm, a width of 530 mm, and with a length equal to L_{ext}. The sidewalls of the channel and chimney are made of Plexiglas plates machined to an accuracy of ±0.03 mm. The whole equipment is in an enclosed room that carefully sealed to eliminate unnecessary air currents, and air drafts were further reduced by vertical screens.

2.1. Numerical model description

For this numerical simulation, the commercial computational fluid dynamics program ANSYS Fluent 19.0 is utilized. Figure. 1 depicts the test section with its boundary conditions and dimensions. This test section is comprised of two vertical plates with a height (L_h) of 100 mm and a depth of 530 mm in the Z-direction. Throughout this simulation, the downstream segment (unheated section extension)'s length L_{ext} changed. As illustrated in Figure.1, the channel spacing and length are b and B, respectively.

The L/Lh=4, B/b=4, and α=10° are used in the current study. Two types of obstructions are inserted inside the heated section as shown in Fig.2. The first obstruction is a rectangular one that has width and height equal to 0.0667 Lh and 0.01335 Lh, respectively. The position of this obstruction is varied according to Table 1. The width and height of rectangular obstructions are 6.67 mm and 1.334 mm, respectively, the second one is a semi-circular obstruction whose center is located at 0.5 Lh. The radius of semi-circular is equal to the width (r = 6.67 mm) of the rectangular one as shown in Fig.2b.The configuration of these obstructions is taken from [7]. The obstructions are inserted to test the m• variation according to these obstructions.

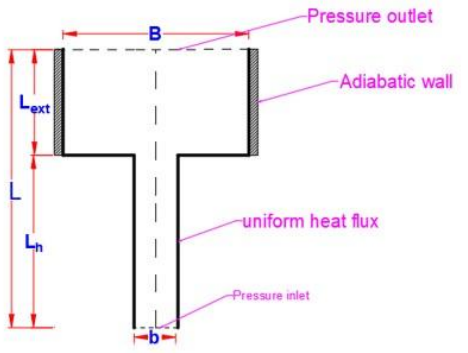

Fig.1. Schematic diagram of the model and its boundary conditions.

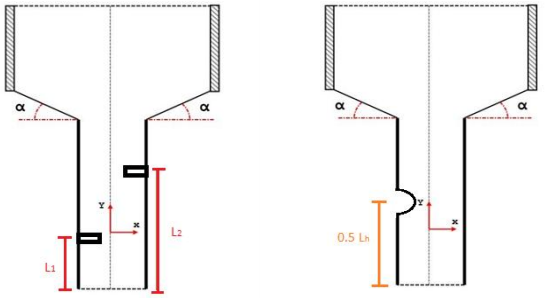

Fig. 2 Schematic diagram for obstruction.

Table 1 Obstructions characteristic length.

Case No.	A	B	C	D
L_1/L_h	0.25	0.25	0.5	0.5
L_2/L_h	0.5	0.75	0.5	0.75

3. Numerical model setup

The air flow inside the channel is considered to be laminar. The viscosity model is used to solve the complex thermal flow field using the Enhanced Wall Function Approach (EWFA) in the near-wall areas in order to meet wall boundary criteria. When the scaled residual of the energy equation reaches 10^{-7} and the scaled residuals of the other equations reach 10^{-4}, convergence is considered. The q" condition is used as the wall boundary condition, whereas equal uniform pressure is required at the chimney's inlet and outflow.

The boundary conditions depicted in Figure 1 may be summed up as follows: 1) Channel inlet is a pressure inlet, 2) Channel exit is a pressure outlet, 3) A constant q" is applied to the channel walls, and 4) the remaining walls are assumed to be adiabatic.

3.1. Assumptions and governing equations.

Two-dimensional, steady-state simulations are conducted. The fluid and solid characteristics are assumed to be fixed in this study. The air characteristics are considered at the fluid flow's mean temperature. In case of laminar flow, the Boussinesq approximation is used, and compression and radiative transport are assumed to be negligible. Thus, the conservation equations governing the fluid could be written in [7]:

Conservation of Mass:

$$\frac{\partial u}{\partial x}+\frac{\partial v}{\partial y}=0 \quad (1)$$

Conservation of Momentum:

$$u\frac{\partial u}{\partial x}+v\frac{\partial u}{\partial y}=v\left(\frac{\partial^2 u}{\partial x^2}+\frac{\partial^2 u}{\partial y^2}\right)-\frac{1}{I?}\frac{\partial P}{\partial x} \quad (2)$$

$$u\frac{\partial v}{\partial x}+v\frac{\partial v}{\partial y}=v\left(\frac{\partial^2 v}{\partial x^2}+\frac{\partial^2 v}{\partial y^2}\right)-\frac{1}{\rho}\frac{\partial P}{\partial y}+g\beta\Delta T \quad (3)$$

Conservation of Energy:

$$u\frac{\partial T}{\partial x}+v\frac{\partial T}{\partial y}=\alpha\left(\frac{\partial^2 T}{\partial x^2}+\frac{\partial^2 T}{\partial y^2}\right) \quad (4)$$

Where, The boundary and initial conditions are: u = v = 0 at the all walls, $T = T_0$ on heated wall, and $T = T_\infty$ as fluid.

3.2. Mesh characteristics.

The model's shape and mesh are created independently by the ANSYS Design modeler and ANSYS MESHER. In the current numerical investigation, a quadrilateral meshing approach with mesh refinement near walls and mesh refinement at the model's sharp edges are employed, as illustrated in Figure 3.

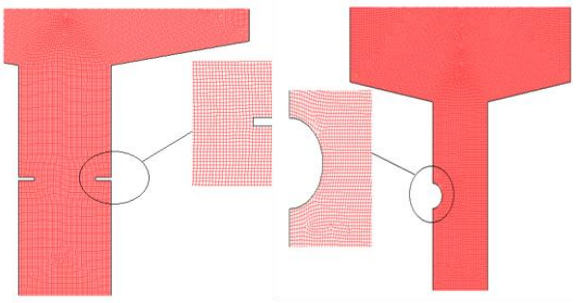

Fig. 3 Mesh shape that employed in the numerical modeling.

As illustrated in Fig 4, the mesh independence test is conducted for each case to confirm the precision of the numerical solution. This graph illustrates the fluctuation of Nux at different mesh sizes, which becomes constant for mesh sizes greater than 102,325. All mesh sizes ranged between 95,456 and 145,569 according to the model dimensions derived from the research parameters. The FLUENT ANSYS documentation recommends this independency test; the initial grid points next to walls are maintained at y+ values between 1 and 5. Grid sensitivity study yielded flow patterns irrespective of the grid.

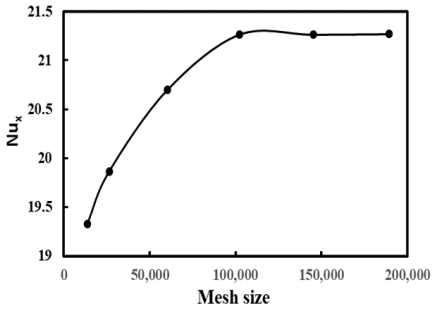

Fig. 4 The value of Nux at different Mesh sizes.

4. Data reduction

Mass flow rate is computed by averaging the upstream and downstream flow rates at the inlet and outlet, using the numerical data. In evaluating the thermal performance of the chimney, Ra is given as [7]:

$$Ra = Gr.Pr = \frac{g\beta q" b^4}{k\upsilon^2}.Pr \qquad (5)$$

where, q" is the convective heat flux, υ is the air kinematic viscosity and β is the expansion coefficient.

The Modified Rayleigh (Ra^{*}) number is represented as:

$$Ra^* = Ra.\frac{b}{L_h} = \frac{g\beta q" b^5}{k\upsilon^2 L_h}.Pr \qquad (6)$$

Dimensionless wall temperature is given by

$$\theta_w = \frac{(T_w - T_\infty)k}{\ddot{q} b} \qquad (7)$$

Local convective heat transfer coefficient (h_x) can be computed with the Nux, for the heated region as:

$$Nu_x = \frac{h_x(x)b}{k} = \frac{1}{\theta_w} \qquad (8)$$

The average value of Nux represents a measure of heat transfer when convection takes place and is calculated as:

$$Nu_a = \frac{1}{L_h}\int_0^{L_h} Nu_x.dx \qquad (9)$$

5. Results and discussion

5.1 Numerical results validation with experimental data.

It is necessary to evaluate validation between experimental and numerical results in order to confirm the correctness of the numerical simulation. Experiments on two-dimensional vertical parallel plates are compared to the numerical findings [7]. Initially, a comparison is conducted to determine the temperature profile of the base case (Lh/b=2.5, L/Lh=1, B/b=∞ and q"=450 w/m^2).

Figure 5 depicts the fluctuation of Θ at various [x/(b/2)] for the basic case; numerical and experimental results for the base case correspond well. The second comparison is made for the situation with the following parameters: Lh/b = 2.5, L/Lh = 1.5, B/b = 3, and q" = 450 W/m2. Figure 6 depicts a comparison between the experimental data reported in [7] and the present test cases for Lh/b=2.5, L/Lh=1.5, B/b=3, and q"=450 W/m2. As demonstrated in Fig. 6, there is a good agreement between the reported experimental data and the numerical model results, with an average error of less than 13 %.

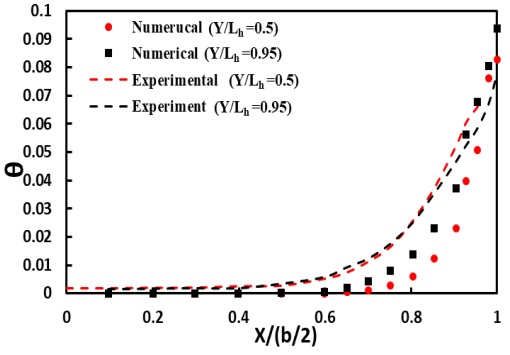

Fig. 5 Temperature profile for base case where α = 0° [7].

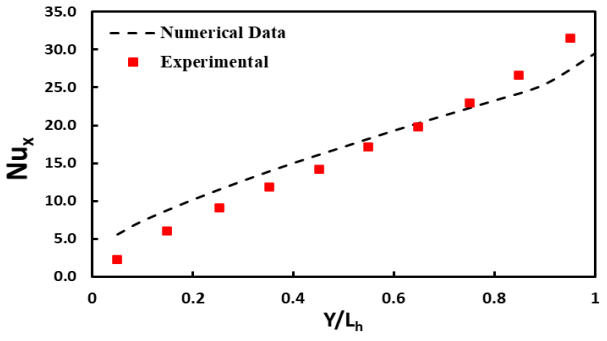

(a)

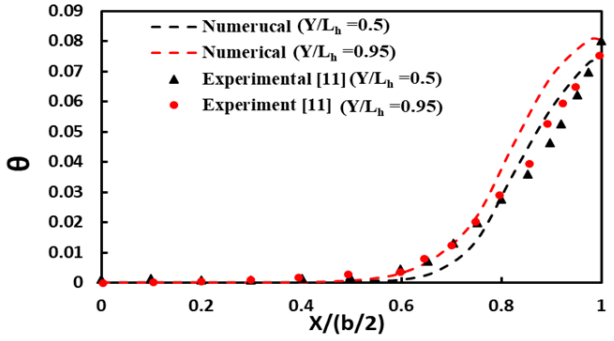

(b)

Fig. 6 Comparison between numerical and experimental results for Temperature profile and Nux where α = 0°.

5.2 Temperature profile and contours

The insertion of obstructions inside the chimney system – in the heated section - reduces the temperature profile of the heated section duo to the disturbance occurs as shown in the following figures. The development of the thermal boundary layer is disturbed by the obstructions, thus the temperature of the surface decreases compared base case as shown in Fig. 7.

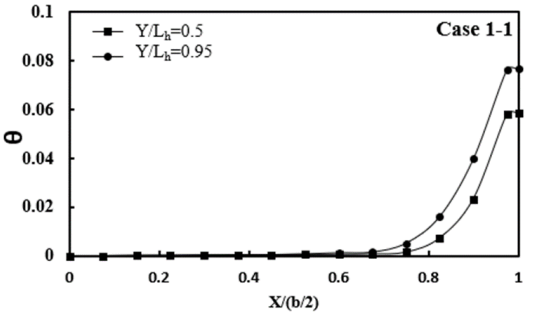

(a)

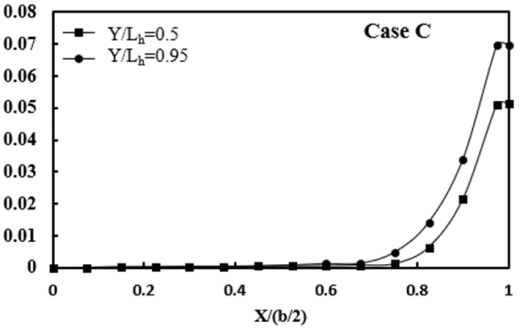

(b)

Fig. 7 Temperature profile of (a) base case and (b) case C.

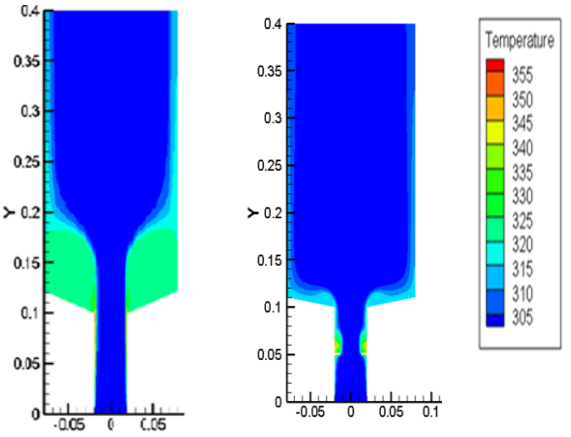

(a) (b)

Fig. 8 Temperature profile for (a) base case and (b) case C.

This figure shows that there is a decrease in the dimensionless wall temperature due to the use of obstruction compared to the base case. In Fig. 8, the thermal boundary layer of base case is better than that for the created one due to obstruction and the disturbance in the fluid flow path.

5.3 Mass flow rate

It is important to note that the insertion of the obstruction inside the heated section leads to a decrease in the mass flow rate because (a) the obstruction make obstacles in the fluid path (b) the obstruction reduces heat transfer rate and that reduce bouncy forces which forces the air to exit.

Figure 9 shows that m• for each obstruction geometry. Results showed that the semi-circular obstruction has the highest m• because it has a smooth round surface compared to a rectangular one. In the rectangular obstruction, the mass flow rate increases when the distance between two obstructions increases and vice versa. As shown in this figure, case 1 in part I has still the highest value of m•, but the semi-circular obstruction has the highest value among obstruction only. It is obvious that the use of any obstruction is not recommend in the chimney system.

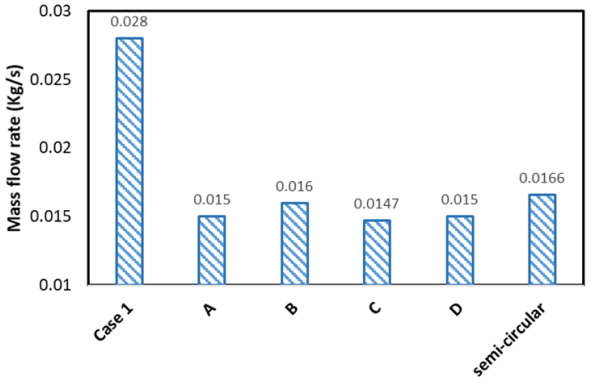

Fig. 9 Mass flow rate for different cases.

5.4 Flow contours.

In Fig. 10, the streamlines with Y-velocity are represented for different obstructions. This figure shows that the obstruction in the fluid path: for rectangular obstruction on both sides: the obstruction throttles the flow and makes vortices behind the obstruction, so the velocity increases which leads to the decrease of upstream. Therefore, m• decreased. For semi-circular obstruction, this obstruction reduces the vortices generation and also throttles the flow. Therefore, the mass flow increased compared to the other obstruction. But still the base case has the highest value due to no obstruction in the flow path and no vortex generation.

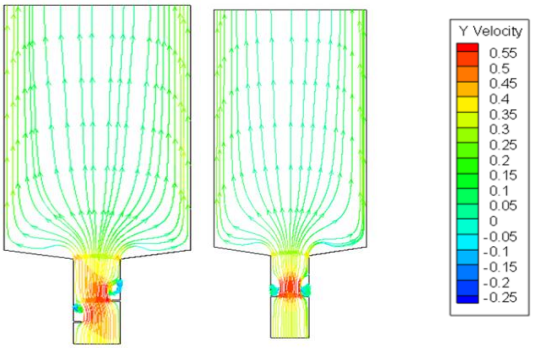

Fig. 10 Velocity profile and streamlines.

6. Conclusion

Numerical simulation was performed on the Chimney system at different parameters to study its effect on the thermal performance and mass flow rate. Different obstructions are inserted in the heated section of the optimum case to study its effect on the performance of the chimney system. Constant heat flux is applied to the channel and the value used is 450 w/m^2.

- Numerical simulation shows the temperature and velocity profiles as well as streamlines.
- Two types of obstruction are used: rectangular and semi-circular at different configurations as mentioned before.
- The dimensionless wall temperature number was reduced for all obstruction chimney duo to obstructions.
- The semi-circular obstruction has the highest value of dimensionless wall temperature number compared to other obstructions, but case 1 has the highest overall cases.
- The obstruction reduces the development of the thermal boundary layer.
- The base case has the highest value of mass flow rate, but the semi-circular chimney has the highest among obstructions.
- The obstructions reduce velocity and form vortex leads to a reduction in mass flow rate.

NOMENCLATURE

b	Channel spacing	m
B	Extension spacing	m
g	Acceleration of gravity	m/s^2
k	Thermal conductivity	w/m. K
L	Total height of the system	m
L_{ext}	Extension height	m
L_h	Heated channel height	m
Nu	Nusselt number	
q"	Heat flux	w/m^2
q_0"	Convergent heat flux	
Ra	Rayleigh number	
Ra*	Modified Rayleigh number	
T_0	Reference temperature	

Greek symbols

θ	Dimensionless temperature
α	Inclination angle

Subscripts

a	average
w	Wall
x	Local
∞	Free stream

References

[1] Kundu B. Semianalytical methods for heat and fluid flow between two parallel plates. J Therm Eng 2015;1:175–81. https://doi.org/10.18186/jte.12495.

[2] Yildiz S. Investigation of natural convection heat transfer at constant heat flux along a vertical and inclined plate. J Therm Eng 2018;4:2432–44. https://doi.org/10.18186/thermal.465654.

[3] Wirtz RA, Stutzman RJ. Experiments on Free Convection Between Vertical Plates With Symmetric Heating. 1982;1:334–45.

[4] Auletta A, Manca O, Morrone B, Naso V. Heat transfer enhancement by the chimney effect in a vertical isoflux channel. Int J Heat Mass Transf 2001;44:4345–57. https://doi.org/10.1016/S0017-9310(01)00064-3.

[5] Da Silva AK, Gosselin L. Optimal geometry of L and C-shaped channels for maximum heat transfer rate in natural convection. Int J Heat Mass Transf 2005;48:609–20. https://doi.org/10.1016/j.ijheatmasstransfer.2004.08.028.

[6] Wang X, Pepper DW. Numerical simulation for natural convection in vertical channels. Int J Heat Mass Transf 2009;52:4095–102. https://doi.org/10.1016/j.ijheatmasstransfer.2009.03.045.

[7] Auletta A, Manca O. Heat and fluid flow resulting from the chimney effect in a symmetrically heated vertical channel with adiabatic extensions. Int J Therm Sci 2002;41:1101–11. https://doi.org/10.1016/S1290-0729(02)01396-0.

[8] Andreozzi A, Buonomo B, Manca O. Thermal management of a symmetrically heated channel-chimney system. Int J Therm Sci 2009;48:475–87. https://doi.org/10.1016/j.ijthermalsci.2008.03.017.

[9] Andreozzi A, Buonomo B, Manca O. Numerical investigation of transient natural convection in a vertical channel-chimney system symmetrically heated at uniform heat flux. Int J Heat Mass Transf 2012;55:6077–89. https://doi.org/10.1016/j.ijheatmasstransfer.2012.06.021.

[10] Manca O, Musto M, Naso V. Experimental investigation of natural convection in an asymmetrically heated vertical channel with an asymmetric chimney. J Heat Transfer 2005;127:888–96. https://doi.org/10.1115/1.1928909.

[11] Chae MS, Chung BJ. Heat transfer effects of chimney height, diameter, and Prandtl number. Int Commun Heat Mass Transf 2015;66:196–202. https://doi.org/10.1016/j.icheatmasstransfer.2015.06.004.

[12] Andreozzi A, Manca O. Radiation effects on natural convection in a vertical channel with an auxiliary plate. Int J Therm Sci 2015;97:41–55. https://doi.org/10.1016/j.ijthermalsci.2015.05.013.

[13] Andreozzi A, Manca O. Thermal and fluid dynamic behavior of symmetrically heated vertical channels with auxiliary plate. Int J Heat Fluid Flow 2001;22:424–32. https://doi.org/10.1016/S0142-727X(01)00080-7.

[14] Kazansky S, Dubovsky V, Ziskind G, Letan R. Chimney-enhanced natural convection from a vertical plate: Experiments and numerical simulations. Int J Heat Mass Transf 2003;46:497–512. https://doi.org/10.1016/S0017-9310(02)00268-5.

[15] Abbas A, Qasrawi F, Wang CC. Investigation of performance augmentation for natural convective heatsink with the help of chimney. Appl Therm Eng 2020;178:115586. https://doi.org/10.1016/j.applthermaleng.2020.115586.

[16] Moon JY, Heo JH, Chung BJ. Influence of chimney width on the natural convection cooling of a vertical finned plate. Nucl Eng Des 2015;293:503–9. https://doi.org/10.1016/j.nucengdes.2015.08.012.

[17] He G. A general model for predicting the airflow rates of a vertically installed solar chimney with connecting ducts. Energy Build 2020;229:110481. https://doi.org/10.1016/j.enbuild.2020.110481.

[18] SLATNİ Y, DJEZZAR M, MESSAİ T. Numerical Investigation of Natural Convection With Heated Tubes in Tunnel Greenhouse. J Therm Eng 2021;7:731–45. https://doi.org/10.18186/thermal.915149.